Control of quantum pathways for the generation of continuous-wave Raman sidebands

Zaitsu, Shin-ichi
PRESTO, Japan Science and Technology Agency (JST)

Imasaka, Totaro
Division of Translational Research, Center for Future Chemistry, Kyushu University |
Department of Applied Chemistry, Graduate School of Engineering, Kyushu University

出版情報：Optics Express. 19 (24), pp.24298-24307, 2011-11-21. Optical Society of America
バージョン：

Control of quantum pathways for the generation of continuous-wave Raman sidebands

Shin-ichi Zaitsu[1,2,*] **and Totaro Imasaka**[1,3]

[1] *Department of Applied Chemistry, Graduate School of Engineering, Kyushu University, 744 Motooka, Nishi-ku, Fukuoka 819-0395, Japan*

[2] *PRESTO, Japan Science and Technology Agency (JST), 4-1-8 Honcho Kawaguchi, Saitama 332-0012, Japan*

[3] *Division of Translational Research, Center for Future Chemistry, Kyushu University, 744 Motooka, Nishi-ku, Fukuoka 819-0395, Japan*

[*] *s-zaitsu@cstf.kyushu-u.ac.jp*

Abstract: The generation of a multifrequency continuous-wave laser through stimulated Raman scattering and phase-matched four-wave mixing in a medium-filled optical cavity is demonstrated. Three different quantum pathways for the four-wave mixing, two of them degenerate and one of them nondegenerate, can be excited independently by tuning the intracavity dispersion. The results suggest that phase-matched Raman sidebands were generated on the longer wavelength side as well as on the shorter wavelength side, which can be used for the Fourier synthesis of a train of ultrashort optical pulses.

OCIS codes: (140.3550) Lasers, Raman; (290.5910) Scattering, stimulated Raman; (190.4380) Nonlinear optics, four-wave mixing; (230.5750) Resonators.

References and links

1. P. D. Maker, R. W. Terhune, M. Nisenoff, and C. M. Savage, "Effects of dispersion and focusing on the production of optical harmonics," Phys. Rev. Lett. **8,** 21–22 (1962).
2. N. Bloembergen and A. J. Sievers, "Nonlinear optical properties of periodic laminar structures," Appl. Phys. Lett. **17,** 483–486 (1970).
3. C. G. Durfee III, St. Backus, M. M. Murnane, and H. C. Kapteyn, "Ultrabroadband phase-matched optical parametric generation in the ultraviolet by use of guided waves," Opt. Lett. **22,** 1565–1567 (1997).
4. C. G. Durfee III, A. R. Rundquist, S. Backus, C. Herne, M. M. Murnane, and H. C. Kapteyn, "Phase matching of high-order harmonics in hollow waveguides," Phys. Rev. Lett. **83,** 2187–2190 (1999).
5. S. Zaitsu, H. Izaki, and T. Imasaka, "Phase-matched Raman-resonant four-wave mixing in a dispersion-compensated high-finesse optical cavity," Phys. Rev. Lett. **100,** 073901 (2008).
6. A. Shirakawa and T. Kobayashi, "Noncollinearly phase-matched femtosecond optical parametric amplification with a 2000 cm^{-1} bandwidth," Appl. Phys. Lett. **72,** 147–149 (1998).
7. M. Zhi and A. V. Sokolov, "Broadband coherent light generation in a Raman active crystal driven by two-color femtosecond laser pulses," Opt. Lett. **32,** 2251–2253 (2007).
8. J. Liu and T Kobayashi, "Cascaded four-wave mixing and multicolored arrays generation in a sapphire plate by using two crossing beams of femtosecond laser," Opt. Express **16,** 22119–22125 (2008).
9. J. L. Silva, R. Weigand, and H. M. Crespo, "Octave-spanning spectra and pulse synthesis by nondegenerate cascaded four-wave mixing," Opt. Lett. **34,** 2489–2492 (2009).
10. F. Benabid, J. C. Knight, G. Antonopoulos, and P. St. J. Russell, "Stimulated Raman scattering in hydrogen-filled hollow-core photonic crystal fiber," Science **298,** 399–402 (2002).
11. M. G. Welch, K. Cook, R. A. Correa, F. Gérôme, W. J. Wadsworth, A. V. Gorbach, D. V. Skryabin, and J. C. Knight, "Solitons in hollow core photonic crystal fiber: engineering nonlinearity and compressing pulse," J. Lightwave Technol. **27,** 1644–1652 (2009).

#149624 - $15.00 USD Received 21 Jun 2011; revised 12 Oct 2011; accepted 13 Oct 2011; published 14 Nov 2011

12. T. Le, J. Bethge, J. Skibina, and G. Steinmeyer, "Hollow fiber for flexible sub-20-fs pulse deliver," Opt. Lett. **36,** 442–444 (2011).
13. R. Ell, U. Morgner, and F. X. Kärtner, J. G. Fujimoto, E. P. Ippen, V. Scheuer, G. Angelow, T. Tschudi, M. J. Lederer, A. Boiko, and B. Luther-Davies, "Generation of 5-fs pulses and octave-spanning spectra directly from a Ti:sapphire laser," Opt. Lett. **26,** 373–375 (2001).
14. A. Bartels and H. Kurz, "Generation of a broadband continuum by a Ti:sapphire femtosecond oscillator with a 1-GHz repetition rate," Opt. Lett. **27,** 1839–1841 (2002).
15. T. M. Fortier, D. J. Jones, and S. T. Cundiff, "Phase stabilization of an octave-spanning Ti:sapphire laser," Opt. Lett. **28,** 2198–2200 (2003).
16. K. Ihara, C. Eshima, S. Zaitsu, S. Kamitomo, K. Shinzen, Y. Hirakawa, and T. Imasaka, "Molecular-optic modulator," Appl. Phys. Lett. **88,** 074101 (2006).
17. J. T. Green, J. J. Weber, and D. D. Yavuz, "Continuous-wave light modulation at molecular frequencies," Phys. Rev. A **82,** 011805(R) (2010).
18. K. Shinzen, Y. Hirakawa, and T. Imasaka, "Generation of highly repetitive optical pulses based on intracavity four-wave Raman mixing," Phys. Rev. Lett. **87,** 223901 (2001).
19. H. Chan, Z. Hsieh, W. Liang, A. Kung, C. Lee, C. Lai, R. Pan, and L. Peng, "Synthesis and measurement of ultrafast waveforms from five discrete optical harmonics," Science **331,** 1165–1168 (2011).
20. Y. R. Shen, *The Principle of Nonlinear Optics* (Wiley-Interscience, 2003).
21. G. P. Agrawal, *Nonlinear Fiber Optics* (Academic Press, 2001).
22. P. A. Siegman, *Lasers* (University Science Books, 1986).
23. S. Zaitsu, C. Eshima, K. Ihara, and T. Imasaka, "Generation of a continuous-wave pulse train at a repetition rate of 17.6 THz," J. Opt. Soc. Am. B **24,** 1037–1041 (2007).
24. S. Zaitsu and T. Imasaka, "Continuous-wave multifrequency laser emission generated through stimulated Raman scattering and four-wave Raman mixing in an optical cavity," IEEE J. Quantum Electron. **47,** 1129-1135 (2011).
25. K. S. Repasky, J. K. Brasseur, L. Meng, and J. L. Carlsten, "Performance and design of an off-resonant continuous-wave Raman Laser," J. Opt. Soc. Am. B **15,** 1667–1673 (1998).
26. R. W. Boyd, *Nonlinear Optics* (Academic Press, 2003).
27. T. J. Kippenberg, R. Holzwarth, and S. A. Diddams, "Microresonator-based optical frequency combs," Science **332,** 555–559 (2011).

1. Introduction

Nonlinear optical interactions rely on the phase-relationship between multiple laser fields coupled to each other through the strongly-driven nonlinear polarization of optical materials. A constant relationship between the phases of the nonlinear polarization and those of the laser fields substantially enhances the energy transfer from one beam to the others in the frequency conversion process; this is known as "phase-matching". The phase-mismatch, Δk, is defined as the difference between wavevectors of the interacting laser fields, and the efficiency of the nonlinear optical interaction is maximized for $\Delta k = 0$. Unfortunately, perfect phase-matching is generally prevented by the chromatic dispersion of nonlinear optical materials that disturbs the phase-relationship during the propagation of the laser fields. To solve this problem, sophisticated techniques based on the use of birefringent crystalline materials [1] and periodically-poled structures [2] are widely used for efficient frequency conversions.

Meanwhile, for the use of isotropic nonlinear optical materials, such as gases, the anomalous dispersion of optical waveguides [3, 4] and negative-dispersive optical cavities [5] can be utilized to improve the efficiency of the frequency conversion. In these methods, the phase-slip caused by the positive dispersion of nonlinear optical materials can be compensated for by the negative dispersion of an optical waveguide or an optical cavity, leading to the extension of the effective coherent length of the nonlinear optical interaction. The generation of deep-ultraviolet ultrashort pulses [3] and high-order harmonics [4] was successfully demonstrated in filled hollow optical waveguides, and a phase-matched nonlinear optical interaction pumped by a low-power continuous wave (cw) was demonstrated in a dispersion-compensated high-finesse optical cavity [5].

To generate broadband radiation through these frequency conversion processes, a large-bandwidth dispersion-compensated region for the phase-matched interactions is required. In

#149624 - $15.00 USD Received 21 Jun 2011; revised 12 Oct 2011; accepted 13 Oct 2011; published 14 Nov 2011

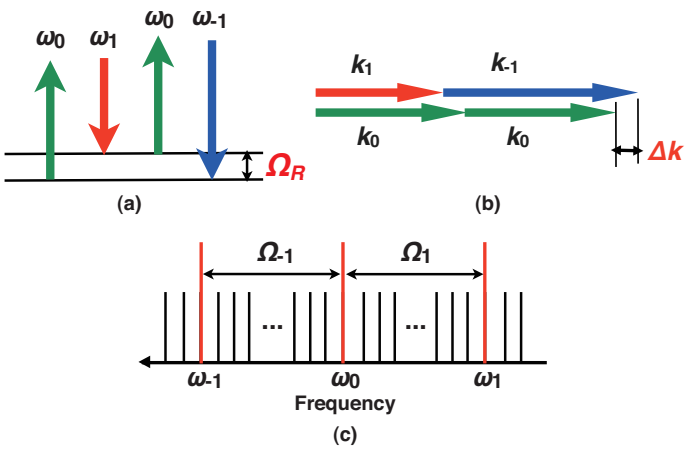

Fig. 1. (a) Energy diagram for coherent anti-Stokes Raman scattering (CARS). ω_0, ω_1, and ω_{-1} are the pump emission, Stokes emission, and anti-Stokes emission, respectively. (b) Phase-mismatch, Δk, for CARS shown in (a). k_0, k_1, and k_{-1} are wavevectors for ω_0, ω_1, and ω_{-1}, respectively. (c) Longitudinal modes responsible for the intracavity CARS.

the case of frequency conversion using solid materials, noncollinear beam geometries allow us to increase the bandwidth for the phase-matching [6–9]. For the use of isotropic gases as nonlinear optical materials, photonic bandgap crystal fibers are a promising tool for broadband frequency conversion [10]. The control of the dispersive properties of hollow-core waveguides by altering the photonic bandgap structure [11, 12] has the potential to achieve broadband frequency conversion, but the bandwidth is still limited at this time. However, the progress in design schemes for negative dispersive mirrors associated with ultrafast laser technology pushes the limit of the tunability of the intracavity dispersion, leading to the generation of mode-locked ultrashort pulses with a bandwidth of greater than one octave [13–15]. Therefore, the dispersion-compensated optical cavity is a promising candidate for the realization of the broadband frequency conversion through the phase-matched processes even when pumped by low-power cw lasers. Such frequency conversions will allow for molecular optical modulators [16, 17] or molecular mode-locked lasers [18] that operate at frequencies of more than 10 THz through the generation of a cw multifrequency laser.

In this paper, the frequency conversion from a single frequency laser into a broadband ($\sim$52.8 THz) multifrequency laser in a high-finesse optical cavity is demonstrated. Broadband compensation of the dispersion of an optical cavity enables us to drive two types of cw-based four-wave mixing, coherent anti-Stokes Raman scattering and nondegenerate four-wave mixing, which involve four single-frequency emission lines. We found that the control of total intracavity dispersion allows us to differentiate the phase-matching conditions for three different pathways in the intracavity four-wave mixing processes. The results suggest that there is phase-matched generation of Raman sidebands on both the shorter and longer wavelength sides, which allows for the Fourier synthesis of a cw-based optical pulse train with an arbitrary waveform [19].

2. Theoretical background

Nonlinear optical interactions in gas-phase media are mainly based on the third-order susceptibility ($\chi^{(3)}$) because of its isotropic nature [20]. Herein, we focus on coherent anti-Stokes Raman scattering (CARS), which is a $\chi^{(3)}$ effect, in a Raman-active gas-phase medium that has a Raman shift frequency of Ω_R between three singe-frequency emissions at a pump emission, ω_0,

#149624 - $15.00 USD Received 21 Jun 2011; revised 12 Oct 2011; accepted 13 Oct 2011; published 14 Nov 2011

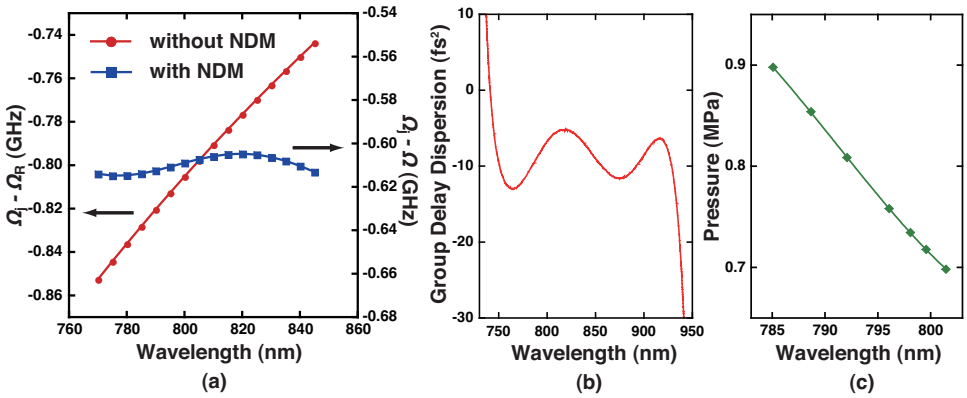

Fig. 2. Dependence of the frequency intervals between the longitudinal modes for ω_0 and ω_1. The solid circles and the solid squares are calculated for an 8-cm-long optical cavity consisting of non-dispersive mirrors and negative dispersive mirrors (NDMs) having a property shown in (b), respectively. Both cavities are filled with hydrogen gas at 750 kPa. Ω_R is the Raman shift frequency of hydrogen, which is assumed to be 17594.79 GHz in this calculation. (b) Wavelength dependence of the group delay dispersion of the NDM used in this experiment. (c) The pressures for the phase-matching condition, $\Omega_{-1} = \Omega_1$, as a function of a wavelength of the pump emission.

a Stokes emission, ω_1, and an anti-Stokes emission, ω_{-1} (see Fig. 1(a)). The phase-mismatch, Δk of CARS is defined by the difference between the wavevectors, i.e. $\Delta k = 2k_0 - k_1 - k_{-1}$, as shown in Fig. 1(b). The efficiency of the process is maximized for phase-matched conditions, i.e. $\Delta k = 0$. This Δk can be expressed using $\Omega_R = \omega_0 - \omega_1 = \omega_{-1} - \omega_0$ and even-order dispersion coefficients, β_{2n} [21]:

$$\Delta k = \sum_{m=2n}^{\infty} \frac{2}{m!} \beta_m \Omega_R . \tag{1}$$

Equation (1) indicates that the compensation of all the even-order dispersion of the medium satisfies the phase-matching condition for the CARS process. When the CARS process is driven in an optical cavity, three longitudinal modes spaced at the frequency of Ω_R interact with each other through the $\chi^{(3)}$-response of the intracavity medium (see Fig. 1(c)). In this intracavity CARS, the phase-matching condition is satisfied when the separation frequencies between these three longitudinal modes are equal, i.e. $\Omega_1 = \Omega_{-1}$ in Fig. 1(c). Unfortunately, the frequency intervals between adjacent longitudinal modes, i.e. the free spectral range (FSR), of a medium-filled optical cavity are not constant as a function of the pump frequency because of the dispersion of the intracavity medium [22]. The frequency dependence of FSR, $\delta\Omega(\omega)$, is calculated by the sum of the contributions of the dispersion given by the intracavity medium and the cavity mirrors:

$$\delta\Omega(\omega) = \frac{c}{2(Ln_g(\omega) + c\beta_{mirror}(\omega))}, \tag{2}$$

where c is the speed of light; n_g is the group refractive index of the intracavity medium; L is the length of the optical cavity; and $\beta_{mirror}(\omega)$ is the group delay given by one bounce of light on the surface of the cavity mirror. Using this $\delta\Omega(\omega)$, the frequency intervals between longitudinal

#149624 - $15.00 USD Received 21 Jun 2011; revised 12 Oct 2011; accepted 13 Oct 2011; published 14 Nov 2011

modes responsible for the CARS (Ω_j, $j = -1, 1$) can be calculated by the following equation:

$$\Omega_j = \sum_{N=N_0}^{N_j} \delta\Omega(\omega_N), \tag{3}$$

where ω_N is the frequency of the Nth longitudinal mode and N_j is the number of the longitudinal mode responsible for ω_j, $j = -1, 0, 1$. The solid circles in Fig. 2(a) show the wavelength dependence of Ω_j for an 8-cm-long Fabry-Perot-type optical cavity filled with hydrogen gas at a pressure of 750 kPa, calculated using Eq. (2) and (3) for $\beta_{mirror}(\omega) = 0$. These plots show that the large wavelength dependence of Ω_j prevents the phase-matching in the CARS process. However, the use of cavity mirrors with negative dispersive properties enables us to compensate for the dependence of Ω_j to satisfy the phase-matching condition of CARS in an optical cavity [5]. Figure 2(b) shows the wavelength dependence of group delay dispersion (GDD) for a mirror with a negative value of GDD from 740 nm to 950 nm, which was used in the following experiment.

The solid squares in Fig. 2(a) represent the dependence of Ω_j on the pump wavelength for the use of a pair of these negative dispersive mirrors (NDMs) as cavity components under the same conditions as for the solid circles in Fig. 2(a). These plots indicate that the compensation of the positive dispersion of the hydrogen gas by the negative dispersion of the cavity mirrors reduces the dependence of Ω_j. Figure 2(c) shows the pressures that satisfy $\Omega_1 = \Omega_{-1}$, i.e. the phase-matching condition, as a function of wavelength when the negative dispersive cavity mentioned above is used. This indicates that the phase-matching condition for CARS in the dispersion-compensated optical cavity can be found from 700 kPa to 900 kPa in the wavelength range from 785 nm to 800 nm.

In the following section, we discuss intracavity four-wave mixing (FWM) processes between the four longitudinal modes of the filled optical cavity shown in Fig. 3(a). In this case, three different quantum pathways of the FWM process shown in Figs. 3(b-d) can be allowed for the pumping frequency of ω_0. The phase-matching conditions of these FWM processes are satisfied when two of the three frequency separations, Ω_{-1}, Ω_1, and Ω_2, are matched: $\Omega_{-1} \neq \Omega_1 = \Omega_2$ (Fig. 3(b)), $\Omega_{-1} = \Omega_1 \neq \Omega_2$ (Fig. 3(c)), and $\Omega_{-1} = \Omega_2 \neq \Omega_1$ (Fig. 3(d)). In the FWM processes shown in Figs. 3(b) and (c), ω_1 and ω_0 are degenerate, respectively, and are called CARS, as mentioned in the previous paragraph. On the other hand, Fig. 3(d) shows a nondegenerate FWM (NDFWM) that involves all four longitudinal modes. Figure 3(e) shows the dependence of Ω_j, $j = -1, 1, 2$, on the frequency of ω_0 for the optical cavity consisting of a pair of the mirrors with negative dispersive properties (Fig. 2(b)), and filled with hydrogen gas at a pressure of 750 kPa. The phase-matching conditions for the three pathways shown in Figs. 3(b-d) are satisfied under the wavelength given at the intersections of the three curves, A, B, and C, which correspond to the pathways shown in Figs. 3(b), (c), and (d), respectively. This predicts that the pathway of the intracavity FWM can be controlled by optimizing the wavelength and the medium pressure in the dispersion-compensated optical cavity when more than four emission lines are involved in the FWM process.

3. Experimental setup

The experimental setup is presented in Fig. 4, which consists of four main parts, a hydrogen-filled high-finesse optical cavity, a pumping laser, coupling optics, and measuring instruments. Negative dispersive mirrors that have the dispersive properties shown in Fig. 2(b) were used as the components of an optical cavity in the following experiment. These mirrors had a reflectivity of >99.96% in the wavelength range from 740 to 920 nm. The optical cavity, which consisted of a pair of these mirrors spaced at 8 cm, was installed in the same type of chamber used in the previous experiment [16, 23]. The chamber was filled with hydrogen gas. The

#149624 - $15.00 USD Received 21 Jun 2011; revised 12 Oct 2011; accepted 13 Oct 2011; published 14 Nov 2011

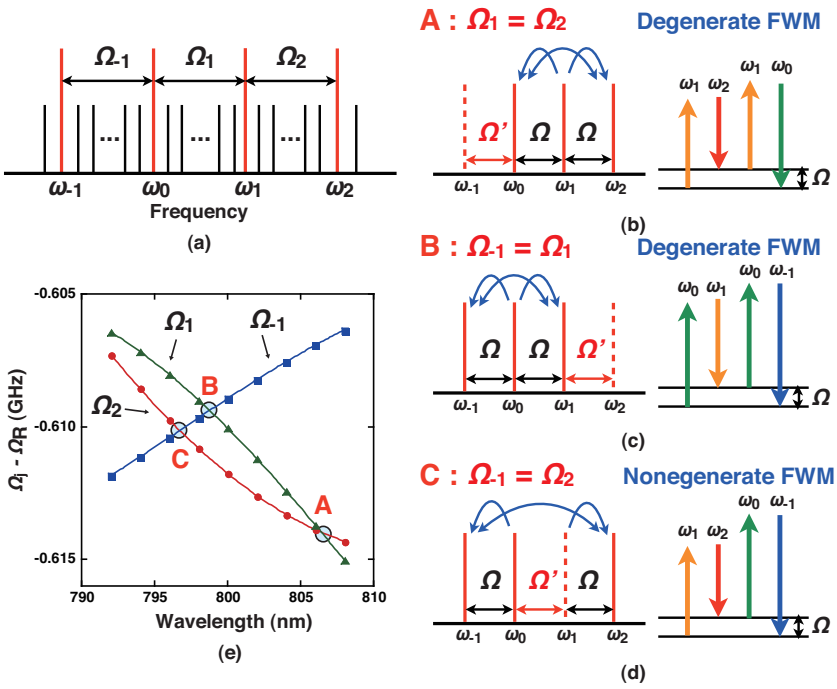

Fig. 3. (a) Longitudinal modes responsible for the intracavity four-wave mixing (FWM) including four emission lines. (b-d) Relationship between longitudinal modes and energy diagrams for FWM processes: (b) the pump frequency of ω_1 is degenerate, (c) ω_0 is degenerate, and (d) nondegenerate FWM including all four emission lines. (e) Dependence of the frequency intervals, Ω_j (j $= -1, 1, 2$) shown in (a) calculated for an 8-cm-long optical cavity, consisting of the NDMs used in this experiment, filled with hydrogen gas at a pressure of 750 kPa.

gas was used as a nonlinear optical medium for the intracavity FWM, which was driven by a single-frequency cw Ti:sapphire laser (Coherent Inc., MBR110, linewidth, <100 kHz, power, 2 W). The laser beam was coupled to the optical cavity through mode-matching lenses to obtain an optimized resonant condition for the enhancement of the intensity of the coupled beam. The frequency of the beam was measured with a wavemeter (Burleigh Inc., WA-1500) and set at ∼800 nm. The hydrogen pressure in the cavity was finely adjusted to determine the phase-matching conditions of the intracavity FWM such that the intracavity medium had a positive dispersion that precisely compensated for the negative dispersion of the cavity mirrors. The intracavity power was controlled by detuning the cavity length slightly from the point at which the intracavity power was maximized [24]. The spectrum of the output beam from the cavity was measured with a spectrometer (Ocean Optics Inc., HR4000) and the dependence of the intensities of the emission lines on the total output power was recorded with LabVIEW Software (National Instruments Inc.).

4. Results and discussions

Figures 5(a) and (b) show the spectra measured for the two different situations that allowed us to generate four emission lines at the maximum output power (∼50 mW): the first anti-Stokes emission (ω_{-1}), the fundamental emission (ω_0), the first Stokes emission (ω_1), and the second Stokes emission (ω_2). The frequency of ω_0 and the hydrogen pressures in the cavity for

#149624 - $15.00 USD Received 21 Jun 2011; revised 12 Oct 2011; accepted 13 Oct 2011; published 14 Nov 2011

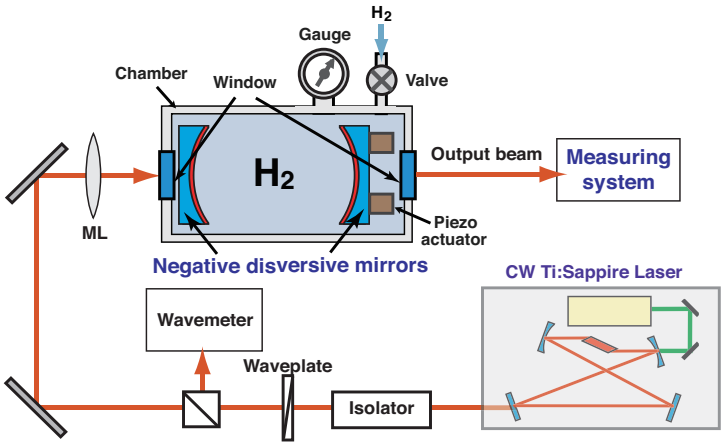

Fig. 4. Schematics of the experimental setup. The high-finesse optical cavity is installed in a stainless-steel chamber equipped with silica windows on both input and output side. The mode-matching lenses (ML) consist of a beam expander ($\times$2.5) and a lens with f = 800 mm. The measuring system includes a beam profiler, a power meter, a spectrometer, and a photo detector. Operating parameters of the cw Ti:sapphire laser and properties of the negative dispersive mirrors are described in text.

obtaining these spectra are shown in the inset of the figures. Figures 5(c) and (d) show the dependence of the intensities of ω_{-1}, ω_1, and ω_2 as a function of the total output power measured for Figs. 5(a) and (b), respectively. Note that there is a difference between the thresholds for the generation of the emission lines. In Fig. 5(c), the threshold for the generation of ω_{-1} coincides with that of ω_1 at 15 mW. The threshold for the generation of ω_2 (30 mW) is larger than this value. However, in Fig. 5(d), the threshold for the generation of ω_{-1} corresponds to that of ω_2 at 20 mW. The threshold for the generation of ω_1 (8 mW) is substantially lower than this value. From Figs. 3(b-d), it can be seen that FWM is a process that generates two photons at the frequencies of the sidebands at the expense of two photons at the fundamental frequency (or frequencies). This leads to the identical thresholds for the generation of the sidebands through the FWM process. Therefore, the coincidence of the thresholds of ω_{-1} and ω_1 in Fig. 5(c) suggests that ω_{-1} was generated through a CARS process that satisfies the phase-matching condition, $\Delta k_0 = 2k_0 - k_1 - k_{-1} = 0$ (Fig. 2(c)). In this case, ω_2 was generated thorough cascaded SRS using ω_1 as a pump frequency. On the other hand, in the case of the FWM shown in Figs. 5(b) and (d), ω_1 was first generated through SRS from ω_0 at 8 mW. Then, the photons of ω_{-1} and ω_2 were generated at 20 mW at the expense of the photons of ω_0 and ω_1 because the phase-matching condition of NDFWM, $\Delta k_0 = k_0 + k_1 - k_{-1} - k_2 = 0$, was satisfied at this fundamental wavelength (800.380 nm) and intracavity pressure (819 kPa). This is the first demonstration of phase-matched NDFWM in an optical cavity driven by a cw laser. In addition, we showed that the dispersion in the optical cavity determined the pathway for the frequency conversion based on $\chi^{(3)}$ nonlinearity.

It was also found that the phase-matching for FWM affected the cascaded SRS for the generation of the high-order Stokes emission in the longer wavelength side. When the pump wavelength was set at 800.355 nm, different behaviors for the generation of ω_2 were observed at different intracavity pressures. Figures 6(a) and (b) show the spectra of the cavity output beam measured at intracavity pressures of 787 kPa and 800 kPa, respectively. Although these two spectra are similar, the thresholds for the generation of ω_2 shown in Figs. 6(c) and (d) are different. Fig. 6(c) shows the typical situation for cw-based cascade SRS in an optical cavity [24],

#149624 - $15.00 USD Received 21 Jun 2011; revised 12 Oct 2011; accepted 13 Oct 2011; published 14 Nov 2011

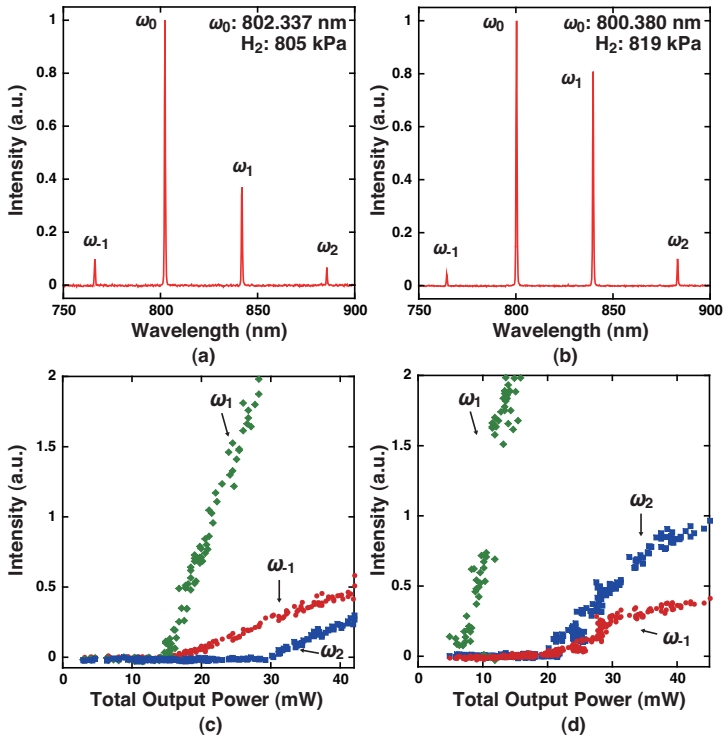

Fig. 5. (a) and (b) Spectra measured at a pump wavelength of 802.337 nm and an intracavity hydrogen pressure of 805 kPa, and at a pump wavelength of 800.380 nm and an intracavity hydrogen pressure of 819 kPa, respectively. (c) and (d) Evolution of intensities of ω_{-1}, ω_1, and ω_2 as a function of the total output power measured under the conditions for (a) and (b), respectively.

in which the threshold for the generation of ω_2 (20 mW) is larger than that of ω_1 (10 mW). On the other hand, Fig. 6(d) shows that ω_2 was first generated at 10 mW, which exactly coincides with the generation threshold of ω_1. Because SRS does not need to satisfy the phase-matching conditions, the threshold power for the Stokes emission through intracavity SRS is determined by the ratio between the Raman gain and the cavity loss, which are independent of the material dispersion [25]. However, FWM affects SRS through Stoke-anti-Stokes coupling for these phase-matching conditions [26]. The coincidence between the thresholds for ω_1 and ω_2 suggests that the phase-matching condition of FWM, $\Delta k = 2k_1 - k_2 - k_0$ (Fig. 3(b)) was satisfied at a pressure of 800 kPa, and hence ω_2 was generated through both the cascade SRS and the phase-matched FWM. With regard to the synthesis of optical pulses, constant frequency intervals are essential for forming a periodical optical pulse train. Raman sidebands generated by SRS in the longer wavelength side can not contribute to the formation of an optical pulse train because of the wavelength variation in the bandwidth of SRS gain [23]. On the other hand, the sidebands generated through parametric FWM process, as shown in Fig. 6(b), can be equally spaced because of the conservation of energy in the frequency conversion process, i.e., $\omega_0 - \omega_1 = \omega_1 - \omega_2$ [27]. This implies that the Raman sidebands measured in Fig. 6(b) are allowed to contribute to the formation of a periodical optical pulse, which should be experimentally demonstrated in the future work by measuring the stability of the waveform synthesized by such phase-locked Raman sidebands.

#149624 - $15.00 USD Received 21 Jun 2011; revised 12 Oct 2011; accepted 13 Oct 2011; published 14 Nov 2011

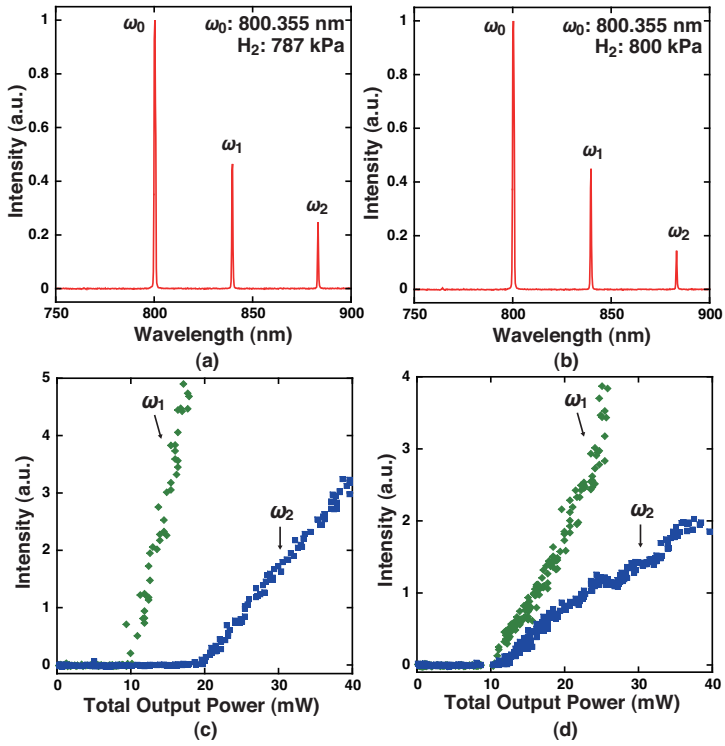

Fig. 6. (a) and (b) Spectra measured at a pump wavelength of 800.355 nm at an intracavity hydrogen pressure of 787 kPa and 800 kPa, respectively. (c) and (d) Evolution of intensities of ω_1 and ω_2 as a function of the total output power measured for the conditions for (a) and (b), respectively.

5. Conclusion

In this paper, we demonstrated the generation of four lines of a single transverse/longitudinal emission via intracavity SRS and phase-matched FWM based on a cw laser. These emission lines arose from two types of pathways: (1) CARS and subsequent SRS, and (2) SRS and subsequent NDFWM. The specific pathway of the intracavity SRS/FWM that occurred depended on the intracavity dispersion to satisfy the phase-matching conditions for each pathway. We also found that the second-order Stokes emission in the SRS process had the same threshold as that of the first-order Stokes emission when the intracavity dispersion was adjusted to a value that satisfies the phase-matching condition of FWM. This suggests that the phase-matched FWM contributed to the generation of the Raman sidebands on both the longer wavelength side and the shorter wavelength side. By synthesizing multiple single-frequency emission lines, these results may lead to the generation of a phase-locked multifrequency cw laser. Subsequently, this system may be used to create a train of optical pulses with a repetition rate of more than 10 THz or an arbitrary waveform.

Acknowledgments

This research was supported by the PRESTO program from the Japan Science and Technology Agency (JST), Grants-in-Aid for Scientific Research, and the Global COE Program, "Science for Future Molecular Systems," of the Ministry of Education, Culture, Sports, Science and

Technology of Japan.

#149624 - $15.00 USD Received 21 Jun 2011; revised 12 Oct 2011; accepted 13 Oct 2011; published 14 Nov 2011